Chapter 2
Review of Relevant Literature

To obtain a clear understanding of secondary flow development, mechanisms of development, and the impact of secondary flows on turbine heat transfer, it is instructive to study past investigations on the topic. This chapter presents a review of past studies that are deemed most relevant to this research effort.

The first section of this chapter discusses various secondary flow models for turbine vane and blade passages that have been proposed in the literature. In addition, the impact of secondary flows on heat transfer, as presented by several researchers, is also examined. In the next section, endwall heat transfer studies with leading edge slot cooling schemes are presented, as the current investigation considers coolant issued through a horizontal, backward-facing slot. The impact of turbine vane inlet conditions on secondary flow development is addressed in the third section of this chapter. Only a few researchers have considered the effects of inlet conditions, with the majority of secondary flow studies being conducted with an isothermal, turbulent boundary layer approach flow. In the final section of this review, methods of secondary flow reduction that have been studied are discussed. Unlike the investigation reported herein, the focus of most secondary flow reduction studies has been to reduce aerodynamic losses in the turbine attributable to these vortical flows. Rather than focusing on the potential aerodynamic benefits, this investigation considered the optimization of a leading edge fillet for maximum thermal benefit.

2.1 Secondary Flow Models and Impact on Endwall Heat Transfer

Many secondary flow models have been proposed in the literature to assist in the visualizing and understanding of the complex flow through a turbine vane or blade passage. In this section, the models that have been most-widely accepted are presented in order of their introduction to the research community. The development of these models is predominantly based on the results of flow visualization with a limited number of flow field measurements being considered.

Though preceded by a few researchers, the work of Langston et al. (1977) is perhaps the first work to draw considerable attention, and clearly the first to present a

visual secondary flow model. Langston et al. studied the three-dimensional flow within a turbine blade passage in a large-scale subsonic cascade with an aspect ratio (span/axial chord) of 0.99. Flow visualization studies were conducted using smoke and ink, while flow velocity and pressure were surveyed in multiple axial planes within the passage using a five-hole pressure probe. Hot-wire measurements were also taken to determine the characteristics of the cascade inlet boundary layer, and to resolve the passage endwall boundary layer flow. The inlet flow to the cascade was a canonical turbulent boundary layer with a disturbance thickness of 3.30 cm (12% span).

The secondary flow model developed from the work of Langston et al. (1977) was later presented by Langston (1980) and is shown in Figure 2.1. This figure shows that as the inlet boundary layer approaches the leading edge of the blade, separation occurs and a horseshoe or leading edge vortex forms. This vortex is characterized by two legs passing through adjacent passages and having opposite sense of rotation. The pressure side leg of the vortex, driven by the cross-passage and radial pressure gradients, merges with passage endwall boundary layer fluid and entrains fluid from the mainstream to form the passage vortex. The other leg of the vortex, labeled the counter vortex due to its opposite sense of rotation, convects around the suction side of the blade and remains in the suction surface-endwall corner. Also shown in Figure 2.1 is the endwall crossflow. This is a result of low momentum passage boundary layer fluid being driven by the strong cross-passage pressure gradient.

A later secondary flow model, shown in Figure 2.2, was presented by Sharma and Butler (1987). In developing their model, Sharma and Butler drew heavily on the work of others, such as Langston et al. (1977), Graziani et al. (1980) and Sieverding (1985), in addition to their own experimental observations. Similar to the description of Langston, the boundary layer entering the cascade separates from the endwall in the leading edge region, and a horseshoe vortex forms. From their own experiments however, Sharma and Butler made an interesting observation, not reported in previous work. Through flow visualization, they observed that while most of the inlet boundary layer gets trapped in the horseshoe vortex system, the fluid closest to the endwall does not become part of the vortex. This fluid was found to be convected toward the suction surface of the airfoil, where it climbs the airfoil surface and exits the cascade above the passage vortex. Since

all of the boundary layer fluid is either trapped in the horseshoe vortex or convected toward the suction surface, it is reasoned that a new boundary layer forms downstream of the separation line created by the leading edge horseshoe vortex. This is consistent with the measurements conducted by Langston (1980), which indicated a much thinner boundary layer in the passage. However, this observed thinning of the boundary layer could arguably be the result of flow acceleration through the passage. While the description of passage vortex development is also similar to that of Langston, Sharma and Butler present a different description of what happens to the suction side leg of the horseshoe vortex. They believe that the suction side leg of the vortex remains near the suction side-endwall corner until the point where the passage vortex intersects the suction surface. At this point, they hypothesized that the suction side leg is forced off the endwall by the passage vortex and begins to orbit the passage vortex. In addition, Sharma and Butler maintain that the orbiting counter vortex retains its identity. They explain the observation of Langston by suggesting that the orbiting suction side leg of the horseshoe vortex coincidentally arrived at the suction side-endwall corner in the cascade exit plane.

Another secondary flow model proposed by Goldstein and Spores (1988) is illustrated in Figure 2.3. Like Sharma and Butler, Goldstein and Spores derived their model not only from their own measurements, but from the flow visualization and measurement results of many investigators including Marchal and Sieverding (1977), Langston (1980), Sieverding (1985), and Sonada (1985). This model includes a number of vortices nonexistent in previous models, and also presents a different view of vortex interactions through the passage. Similar to previous models, this model acknowledges the development of a leading edge or horseshoe vortex, and attributes vortex development to the pressure variation at the airfoil leading edge. Due to the boundary layer velocity distribution and stagnation of the flow at the leading edge, the flow is forced down toward the endwall and rolls up into the horseshoe vortex. The effect of the cross passage pressure gradient on the pressure side leg of the leading edge vortex and subsequent passage vortex development also remains the same as previous work. Two differences of this model occur downstream of the location where the endwall separation line intersects the airfoil suction surface. Goldstein and Spores present the passage

vortex as lifting off the endwall upon reaching the suction surface at the point of minimum static pressure. In addition, they indicate lift off of the suction side leg of the horseshoe vortex at the endwall separation line. Unlike Sharma and Butler's orbiting vortex model, Goldstein and Spores believe that the suction side vortex leg continues through the passage along the suction surface and above the passage vortex. These lift off phenomena are attributed to higher velocities and lower pressures located away from the passage endwall-suction surface corner. Another major difference of this model is the inclusion of a series of small corner vortices. Two of these corner vortices are shown to develop at the leading edge due to the action of the leading edge vortex. Their sense of rotation is opposite that of the corresponding horseshoe vortex leg. A third corner vortex is shown to originate in the pressure surface-endwall corner due to the downwash of fluid onto the endwall in this region. Finally, a pair of counter-rotating corner vortices is shown to originate just downstream of where the passage vortex lifts off the endwall. The generation of this pair of vortices is attributed to an interaction of the passage vortex and the airfoil suction surface. It is important to note that the presence of many of these vortices was inferred from endwall mass transfer measurements using the naphthalene sublimation technique. There have been no reported direct flow field measurements quantifying these vortices.

A more recent secondary flow model found in the literature is that presented by Takeishi et al. (1990) and illustrated in Figure 2.4. Like all previous models, the inlet boundary layer is shown to roll up into a leading edge horseshoe vortex, and the passage vortex is shown to be the dominant element of the flow. Development of the passage vortex is also explained in a similar fashion to previous models, with the pressure side leg of the leading edge vortex forming the core of the vortex. The endwall separation line is presented as defining the furthest extent into the passage that the inlet boundary layer penetrates. Downstream of the separation line, a new endwall boundary layer forms. Associated with this line of separation, the migration of inlet boundary layer fluid toward the suction surface is explicitly shown (crossflow "A"). Similar to the model of Goldstein and Spores, Takeishi et al. indicate that the suction side leg of the horseshoe vortex, which they label the counter vortex, lifts off the endwall and remains above the passage vortex through the passage. However, no indication of passage vortex lift off is

given. Other differences relative to the model of Goldstein and Spores are the absence of leading edge and pressure side corner vortices and the presence of a single suction side corner vortex rather than a vortex pair. The sense of rotation of the corner vortex presented by Takeishi et al. is opposite that of the passage vortex.

Though there are differences between the models discussed, there is general agreement on the predominant features of the secondary flow field and what drives their development. The horseshoe vortex forms due to the spanwise pressure variation resulting from boundary layer stagnation at the airfoil leading edge. The passage vortex forms due to the amplification of the pressure side leg of the horseshoe vortex by cross-passage boundary layer flow. As for the features of the flow that were not agreed upon, no conclusive result can be drawn without detailed flow field measurements. Differences between the secondary flow models may be the result of flow field dependence on geometrical features, such as turning angle and leading edge radius, and inlet conditions. Flow field measurements performed in the turbine vane cascade that was used in this investigation indicate agreement with the model presented by Langston (Kang and Thole, 2000). The importance of understanding secondary flows and their development is due to the impact of such on turbine heat transfer, which is discussed next.

In the development of gas turbines, detailed knowledge of local surface heat loads is desirable and would be instrumental in the design process, however, obtaining such data, especially with a high degree of resolution, remains a difficult task. Accurate predictions of heat transfer are also difficult to make given the highly complex, three-dimensional flow fields that arise due to secondary flows. In order to determine the effects of secondary flows on heat transfer, many researchers have adapted their experimental facilities to accommodate heat transfer measurements. In this section, the effect of turbine passage secondary flows on heat transfer, as presented by several researchers, will be reviewed.

The first significant work regarding secondary flow effects on heat transfer was presented by Graziani et al. (1980). In this study, local heat transfer rates on the endwall, suction, and pressure surfaces of a large-scale turbine blade cascade were measured for two different inlet boundary layer thicknesses, ~15% and ~2% span, and a Reynolds number characteristic of gas turbine operation. The turbine blade geometry used in this

study was the same as that used by Langston et al. (1977). Graziani et al. determined that the passage vortex, the size of which was dependent on the inlet boundary layer thickness, is instrumental in determining the overall flow field and thus heat transfer through the blade passage.

To determine the effect on the flow field, surface flow visualization and pressure field measurements were taken for both inlet boundary layer thicknesses. From these measurements, it was determined that the inlet boundary layer thickness affects the size of the horseshoe vortex as well as the size and position of the passage vortex. From surface flow visualization, the region of influence of the leading edge vortex was shown to be smaller for the thin inlet boundary layer. The indication of this was the location of the saddle point of separation, which was shown to be closer to the blade surface and further into the passage for the thin inlet boundary layer. Indication of the size and influence of the passage vortex was also taken from flow visualization on the suction surface of the blade. Again, the thicker inlet boundary layer resulted in a larger passage vortex as indicated by the convergence of suction surface streamlines toward the blade midspan. The streamlines were shown to converge further toward midspan for the thick inlet boundary layer. Measured suction surface pressure distributions were consistent with the flow visualization results, indicating stronger three-dimensional flow for the thick boundary layer case. Flow visualization results were not presented for the pressure surface as no significant three-dimensional features were observed. The pressure contours presented for the pressure surface confirm the two-dimensional character of the flow over the surface.

In addition to the flow visualization and pressure measurements, heat transfer measurements were also taken on the endwall and blade surfaces by Graziani et al. Through application of a uniform surface heat flux and measurements of surface temperature at discrete locations, contours of Stanton number were calculated over the passage surfaces. Several regions of high heat transfer were observed on the passage endwall and can be directly attributed to secondary flows. One such region is near the blade leading edge, where the horseshoe vortex develops. Consistent with the flow visualization results, the region influenced by the vortex is larger for the 15% span inlet boundary layer relative to the 2% span boundary layer case. A second region of high

endwall heat transfer is observed adjacent to the suction surface downstream of the passage throat. Interestingly, this second region of high heat transfer is much more pronounced for the thin inlet boundary layer. To explain the augmented heat transfer observed for the 2% span boundary layer, it is suggested that the passage vortex resides closer to the endwall for this case. Supporting this explanation, contours of Stanton number on the blade suction surface indicate that the passage vortex does indeed reside close near the endwall for the thin boundary layer. In addition, the corresponding contours for the thick boundary layer case indicate that the passage vortex moves away from the endwall and up the suction surface. The last region of high endwall heat transfer resides downstream of the blade trailing edge. Characterized by similar levels of heat transfer for both inlet cases, this region is not directly attributed to passage secondary flows.

A second study of importance is the work of Gaugler and Russell (1984). Similar to the investigation of Graziani et al., Gaugler and Russell performed flow visualization studies of passage secondary flows and compared their results with the endwall heat transfer measurements of Hylton et al. (1981). The objective of this study was to investigate the correlation of observed flow patterns with the previously reported endwall heat transfer patterns. Flow visualization was performed using neutrally buoyant helium bubbles, smoke from oil-soaked cigars, and a surface ink dot technique.

Correlation of the flow visualization data with endwall heat transfer was observed in several regions of the endwall. The most obvious correlation was in the leading edge region, where the horseshoe vortex causes a local peak in Stanton number. A smaller peak in Stanton number was shown to occur in the region where the three-dimensional endwall separation line intersects the suction surface of the turbine vane. In this region, surface flow visualization indicated that the endwall flow begins to climb onto and up the vane suction surface. Finally, another peak in Stanton number was observed downstream of the vane trailing edge, but no relationship to the passage secondary flows could be drawn. This peak was also observed by Graziani et al.

The final study of importance is that of Kang, Kohli and Thole (1999). In this investigation, flow field measurements were taken in the leading edge stagnation plane of the same turbine vane used in the study reported herein. In addition to flow field

measurements, high-resolution endwall heat transfer measurements were taken throughout the passage. The results for two different vane exit Reynolds numbers were compared to determine the effect of this parameter on the flow in the leading edge region and on endwall heat transfer. For both Reynolds numbers, formation of a leading edge horseshoe vortex was observed. Consistent with the observations of other researchers, the location of the endwall separation line was shown to be closer to the vane for the high Reynolds number case. Similar to the observation of Gaugler and Russell, a local peak in Stanton number was observed at the vane leading edge as a result of horseshoe vortex development. The effect of the passage vortex was also apparent with a general increase in endwall heat transfer through the passage.

In all the investigations discussed above, the importance of passage secondary flows on heat transfer was illustrated. The vortex action associated with these flows can substantially augment heat transfer at the surface of turbine components, resulting in premature failure. For this reason, it is important to combat the formation of these flows and the associated regions of high heat transfer in the design of modern turbines.

2.2 Endwall Heat Transfer Studies with Slot Cooling

Driven to achieve higher cycle efficiency and specific power output, the gas turbine industry is continually increasing turbine inlet temperature resulting in thermal loads that threaten the durability and operational life of turbine components. To sustain operational life and turbine durability, turbine thermal designers are continually investigating new and innovative ways to cool components. Secondary flow structures as discussed in the previous section complicate the job of these designers especially in regard to providing adequate thermal protection in the endwall regions of a turbine passage. Surface film cooling, in which cool air is injected through strategically placed holes on the flow surfaces, is a common technique employed to protect turbine components from excessive heat load. However, this technique often falls short due to the strong influence of the secondary flow field.

Another method of providing thermal protection to the endwall and near-endwall surfaces that has received attention is that of coolant injection at the combustor/turbine interface. Traditionally, the combustor and high-pressure turbine nozzles are designed

and manufactured separately resulting in the issue of joining the two. Typically a gap or slot results at the interface due to mismatch in thermal expansion between the combustor and first vane. To avoid ingestion of hot combustion gases into the resultant joint, combustor bypass air is typically permitted to flow through the joint in the form of an engineered leak. Naturally, the usefulness of this coolant flow in providing thermal protection to the vane passage endwall came into question. As this cooling technique is employed in the current investigation, this section presents a review of research efforts in this area.

Perhaps the first investigation of significance regarding slot cooling is that of Blair (1974). Blair measured the convective heat transfer coefficient and film-cooling effectiveness distribution on the endwall of a vane passage with slot coolant injection directly upstream of the leading edge. The test facility consisted of a single curved passage whereby the static pressure distributions on the suction and pressure surfaces were set by adjustment of exit tailboards and leading edge bleed flow slots. Two different endwall test surfaces were employed in the investigation: a nearly adiabatic surface constructed of one inch thick urethane foam for determination of adiabatic effectiveness, and a test surface comprised of individually-controlled heating elements for determination of heat transfer coefficient distribution. The injection angle for the coolant was 30°, and measurements were performed for three different slot blowing ratios, as well as for the case of no slot flow.

The results of Blair's adiabatic effectiveness tests showed extended cooling near the suction side corner and reduced cooling near the pressure side corner. These observations indicate the presence of and influence of cross passage secondary flow on the injected coolant. The cross passage flow transports coolant from the pressure side to the suction side, resulting in an accumulation of coolant in the suction-side corner. The extent of endwall cooling was observed to increase with increased slot cooling flow. With no coolant injection, slightly elevated levels of heat transfer were observed near the vane leading edge due to the presence of the leading edge vortex. In the downstream third of the passage, a region of maximum heat transfer was observed adjacent to the suction-endwall corner. This maximum is believed to be the result of the passage vortex. For testing with coolant injection, heat transfer coefficients near the vane leading edge

were slightly less than those for no coolant injection, however, immediately downstream of the injection slot, heat transfer was observed to be larger. The maximum heat transfer coefficient in the downstream third of the passage was approximately 10 percent less than that measured for the no slot flow case. The location of the maximum was essentially unchanged. These results indicate that the passage secondary flows are relatively unaffected by coolant injection upstream of the vane leading edge.

Roy et al. (2000) also investigated the use of leading edge slot cooling both experimentally and computationally. Experiments were carried out in a low-speed linear cascade of five turbine vanes. The slot configuration, for which no detailed description was given, appears to consist of three closely-spaced adjacent slots centered about the vane leading edge. The three slots extend approximately a quarter pitch to either side of the vane leading edge, unlike the continuous slot configuration tested by Blair (1974). The angle of injection is relatively shallow at 20°. Only one blowing ratio of 1.3 was considered in this investigation.

The results of Roy et al. indicated that without slot coolant injection there are regions of elevated heat transfer about the leading edge and in the downstream half of the vane passage. Interestingly, the highest measured values of heat transfer about the leading edge occur at the suction side shoulder of the vane and are attributed to an intense corner vortex. The downstream region of elevated heat transfer is similar to that observed by Blair and others, and is attributed to the presence of the passage vortex. The Reynolds number based on axial chord for this test was relatively low in comparison to typical engine operating conditions. Heat transfer results for the corresponding computational simulation agreed quite well with the experimental measurements.

With the addition of slot cooling flow, Roy et al. found that endwall heat transfer was reduced considerably in the leading edge region as well as along the vane pressure surface in the downstream half of the passage. Results of endwall cooling effectiveness measurements indicate good thermal protection about the leading edge and in the pressure surface/endwall corner through the passage. Contrary to the results of Blair and others, Roy et al. did not observe cross passage transport of the coolant, leaving a region of thermal vulnerability along the suction surface with high heat transfer and low

effectiveness. The lack of cross passage coolant transport is inexplicable and warrants further investigation.

The effects on cooling performance of slot bleed injection over a contoured endwall through a vane passage was investigate in a two-part study by Burd and Simon (2000) and Burd, Satterness, and Simon (2000). The former of these two studies presents the effects of slot bleed flow on the flow field and overall total pressure loss through the cascade, while the latter study presents the effects on the thermal field. The experimental setup for both investigations is essentially the same, consisting of a two-passage, three airfoil, large-scale, high pressure turbine nozzle cascade preceded by a combustor simulator that produces high-level(~9%), large-scale(14-19% C) turbulence. The cascade features one flat and one contoured endwall contracting through the vane passage. Located 0.1 axial chord upstream of the vane leading edge, combustor bleed cooling flow is injected through near-continuous, angled slots at bleed-to-core mass flow ratios ranging from 0 to 6%. The width of the slot was 2.5% C, the length to width ratio was 4.0, and the injection angle was 45°.

In the first of these two studies, Burd and Simon (2000) performed detailed flow field measurements upstream of the cascade, at the exit of the slot, near the exit of the passage, and downstream of the cascade. A single-sensor hot-wire was utilized for characterizing the flow entering the cascade and for measuring the pitchwise non-uniformity of slot injection at varying bleed-to-core mass flow ratios. Substantial non-uniformity of slot exit velocity was reported for the lowest coolant flow rate, and is attributed to the non-uniform pressure field created as the core flow encounters the vane cascade. The non-uniformity in exit velocity was observed to diminish with increasing slot mass flow, with the lowest slot exit velocities consistently occurring at a pitchwise location coincident with the vane stagnation.

A triple-sensor, hot-film anemometer was used to perform flow field measurements near the exit plane of the cascade at the 90% axial chord location. At low coolant mass flow rates, two secondary flow structures along the vane suction surface, one near each suction/endwall corner, were indicated as distinct regions of streamwise momentum deficit. These structures are believed to be the familiar passage vortices. With increased bleed flow exiting the slot, the secondary flow structure adjacent to the

contoured endwall was progressively suppressed and observed to move into the suction/endwall corner. Burd and Simon believe the slot flow provides streamwise momentum that thins the boundary layer and weakens the cross-flow that aids in the formation, growth, and propagation of the secondary flow structure.

The final series of flow field measurements performed by Burd and Simon were aimed at determining the effect of slot coolant injection on the total pressure loss through the vane cascade. The results of these measurements indicate that injection has little to no impact on the overall total pressure loss. Burd and Simon viewed this finding as significant, as this cooling configuration shows promise of providing thermal protect with negligible aerodynamic penalty.

The second study in this series, Burd, Satterness, and Simon (2000), investigates the thermal performance of the leading edge slot cooling scheme. For this study, two different contoured endwall test surfaces were employed: one fabricated from low thermal conductivity phenolic for adiabatic testing, and another geometrically-identical one made of aluminum for heat transfer testing.

In the adiabatic tests, the distribution of coolant through the passage for various bleed-to-core mass flow ratios was measured utilizing temperature as a tracer. Thermocouple probes of different lengths and shapes to accommodate local passage geometry were used for measurement of temperature distributions in several axial planes through the cascade. At lower values of bleed-to-core mass flow ratio(BFR $\leq$ 2.0%), the injected coolant was found to be strongly influenced by endwall cross-passage flow, resulting in the accumulation of coolant near the suction/endwall corner and a lack of thermal protection in the pressure/endwall corner. At higher values of BFR($\geq$ 3.2%), the injected coolant was observed to provide better uniformity of coverage to the contoured endwall with coolant supply to the pressure/endwall corner. The best overall endwall thermal protection was provided at a BFR = 3.2%, as values of BFR in excess of this result in diminishing suction/endwall corner coolant coverage. It is theorized by Burd, Satterness, and Simon that the increased streamwise momentum of the injected coolant decreases the susceptibility of this flow to be influenced by the passage cross-flow.

For the heat transfer tests, Burd et al. replaced the phenolic endwall with a near-isothermal, heated aluminum replica. Local values of heat transfer coefficient were

determined at only a few locations through measurement of near-wall temperature gradients using a thermocouple probe based on the design of Blackwell and Moffat (1975). The injected slot flow was observed to increase heat transfer near the vane leading edge, while through the passage augmentation progressively approached unity. Overall, coolant injection had little net impact on endwall heat transfer. Fortunately, regions of highest augmentation were found to coincide with those of high cooling effectiveness, yielding a prediction of net heat flux reduction.

A companion study to those described above was conducted by Oke at al. (2000), in which the near-continuous coolant slot was replaced by two staggered rows of discrete film holes. In comparison with the results for slot injection, higher mixing was observed with discrete hole injection with an associated drop in cooling performance of approximately 20-30%. As with slot injection, the streamwise momentum of the injected coolant was found to be paramount in avoiding the accumulation of coolant in the suction/endwall corner.

Another two part investigation of slot cooling was reported by Colban et al. (2003a) and Colban et al. (2003b). In the former study, these researchers examined the effect of varying both the amount of slot flow and the amount of combustor liner film-cooling on the endwall adiabatic effectiveness levels for a first vane, while in the latter study, the effects of coolant flow variations on the flow and thermal fields in the turbine cascade are investigated. The experimental facility utilized consists of a large-scale vane cascade preceded by a like-scale combustor simulator as described in Chapter 4 of this document. Unique to this investigation is the injection of coolant through a backward-facing slot, unlike the flush slots of many previous studies, and the inclusion of combustor coolant flow in the experimental model.

In the first study by Colban et al. (2003a), the effects of varying both combustor liner cooling flow and slot cooling flow on endwall adiabatic effectiveness levels were investigated. The inclusion of combustor liner cooling in this study was based on the premise of determining the relative value of this cooling flow for endwall thermal protection. The researchers are quick to point out however, that varying the combustor liner cooling flow not only impacts endwall effectiveness levels, but also alters the spanwise total pressure profile entering the vane cascade. Furthermore, this total pressure

profile determines the secondary flow field, thus, it is essential that experimental results are viewed in light of this. Five different test cases were selected for investigation and are described according to their resultant total pressure profiles. A nominal test case was characterized by a near-wall peak in the total pressure profile as measured above the horizontal slot. A case with reduced combustor coolant flow and a case with increased combustor coolant flow resulted in a flatter total pressure profile and a more highly peaked profile, respectively. To investigate the influence of the slot coolant flow, the nominal slot flow rate was halved and doubled. While perturbing the slot flow does not alter the total pressure distribution measured above the slot, the total pressure of the slot flow itself changes.

The experimental results of Colban et al. suggest that an optimum combustor cooling flow rate exists, beyond which thermal benefit to the vane endwall diminishes. This observation is explained by the fact that increasing the combustor cooling flow leads to an increased peak in the total pressure profile entering the vane passage. It is theorized by these researchers that the resulting stronger secondary flows undermine the effectiveness of the cooling flow. In contrast, experimental results of varying slot cooling flow indicate a continual increase in endwall effectiveness with increasing flow. By increasing the slot cooling flow, the associated total pressure increases, thereby reducing the driving potential for the secondary flow. Through this mechanism, endwall adiabatic effectiveness values improve with increased slot blowing.

In the second part of this investigation, Colban et al. (2003b), the thermal and flow fields associated with the various test cases were examined. The most significant result of this study is the demonstrated influence of the inlet total pressure distribution on the secondary flow field throughout the vane passage. Unlike past investigations that assumed a simple two-dimensional turbulent boundary layer profile entering the first vane, this study presents the first experimental measurements for a more realistic combustor exit profile, and provides undisputable evidence of the importance of properly modeling inlet conditions. Laser Doppler velocimetry measurements were performed in two selected flow planes in order to visualize the local secondary flow fields.

The first plane considered by Colban et al. extends directly upstream of the vane stagnation and is thus referred to as the stagnation plane. Flow field measurements in this

plane illustrate the interaction of the approaching flow with the vane leading edge and the early development of secondary flow structures. For nominal flow conditions, the measured stagnation plane flow field is characterized by a flow split and a flow impingement. The flow split occurs at a spanwise location coincident with the near-wall peak in total pressure. At this location, the flow is driven both up toward the midspan and down toward the endwall due to lower total pressure in these regions. The down-turning of the flow is indicative of leading-edge horseshoe vortex development, while the up-turning of the flow is a newly-observed phenomenon. The reason for this up-turning of the flow as well as the observed flow impingement is the presence of a local total pressure minimum between the flow split and midspan. Not surprisingly, the spanwise location of flow impingement was coincident with the local minimum in total pressure.

Flow field measurements in a second analysis plane considered by Colban et al., located in the vane passage and extending normal to the vane suction surface, illustrate the full ramifications of that observed in the stagnation plane. The secondary flow field in this plane is characterized by the presence of an addition vortex rotating counter to the passage vortex. The development of this vortex is attributed to the inlet total pressure profile, specifically the local minimum in total pressure that occurs between the near-wall maximum and midspan. The presence of this additional vortex reiterates the importance of properly modeling realistic boundary conditions.

A final series of investigations involving slot cooling were reported by Kost and Nicklas (2001) and Nicklas (2001). These studies examined endwall film-cooling in a transonic vane cascade employing both slot coolant injection upstream of the vane leading edge, and discrete film hole coolant injection in the passage. Aerodynamic measurements indicated a reduction in endwall cross flow and passage vortex strength with both slot and film hole coolant injection. Slot injection, however, was found to dramatically strengthen the horseshoe vortex. This strengthening of the horseshoe vortex was attributed to the slot being located in the region of the saddle point upstream of the vane. To prevent such strengthening, it was suggested that the slot be repositioned further upstream. Heat transfer measurements concur with the aerodynamic results, indicating a strong increase in endwall heat transfer coefficient in the leading edge region with slot cooling versus without slot cooling. Despite this observed increase in the heat

transfer coefficient, results of endwall adiabatic effectiveness measurements indicate high effectiveness values in the upstream part of the passage attributable to slot cooling flow. No input regarding the net effect on endwall heat load was provided for this investigation.

2.3 Effect of Inlet Conditions on Secondary Flows

In most studies of secondary flow development and turbine aerodynamics, uniform inlet radial temperature profiles and two-dimensional boundary layer velocity profiles have been assumed to simplify experimentation and analysis. However, these profiles are not representative of the actual conditions that exist at the entrance to a turbine. In an actual engine, significant radial and circumferential variations in flow temperature and total pressure exist at the exit of the combustor. The importance of properly modeling these conditions is emphasized by the work of Colban et al. (2003a) and Colban et al. (2003b), presented in section 2.2 of this chapter. The results of these researchers indicate that the inlet conditions to the turbine, specifically the inlet total pressure profile, influence the secondary flow pattern that develops. Furthermore, the secondary flows were found to strongly affect the distribution and effectiveness of coolant, as well as, the redistribution of the thermal field through the vane passage. In engine development today, especially military engine development where the limit of turbine inlet temperature is continually challenged, poor prediction of the secondary flows in a vane or blade passage can result in local hot spots on flow surfaces that dramatically reduce the life of turbine components. In this section, several investigations concerning the effects of non-uniform inlet profiles on turbine passage flow are discussed.

The first investigation of significance was that of Schwab, et al. (1983), undertaken at the NASA Lewis Research Center in the early 1980's. In the experimental portion of the study, non-uniform inlet radial temperature profiles were generated using a specially designed inlet section to a 0.767 scale model turbine. This turbine inlet section was given the acronym CERTS, meaning Combustor Exit Radial Temperature Simulator. The results of total temperature and total pressure radial surveys at the vane inlet and rotor exit were presented for both a non-uniform and a uniform inlet temperature profile.

Analysis was performed with a three-dimensional time-marching inviscid rotational flow code, using the experimentally measured inlet profiles as the inlet boundary condition. Contour plots showing the distortion of the inlet temperature profile were presented in addition to plots of temperature seen by the metal. Vector plots of the calculated secondary flows were also presented.

The primary results of interest of Schwab, et al. are those of the analysis. Computed secondary flow vectors in the vane passage illustrate the migration of mainstream fluid along the pressure surface toward the hub and tip endwalls. The effect of these secondary flows is evident in the calculated temperature distribution at the exit to the vane. Temperature contour plots show distortion of the relatively flat inlet isotherms along the pressure surface, resulting in elevated metal temperature at the pressure side hub and tip. Similar results are presented for the blade passage. Due to the measurement limitations in a rotating high speed facility, experimental verification of the analysis results was not possible.

The fundamental limitation of this study by Schwab, et al. was the inviscid analysis code utilized. Prediction of secondary flows without modeling the effects of viscosity does not present the entire picture, however, despite this simplifying assumption, this study clearly illustrates that secondary flows cause the redistribution of flow and temperature. Gaining an understanding of this phenomenon would be instrumental in the design of turbines for extended life.

Another more recent computational study on the effects of inlet conditions on secondary flows was performed by Hermanson and Thole (2000). In this study, the flow field through a modern turbine vane was modeled for different inlet boundary profiles of temperature and velocity. A commercial computational fluid dynamics software package called Fluent was utilized in the investigation. After qualifying the computational code through a comparison to experimental results for a baseline case, the vane passage flow field was computed for different inlet profiles and the resulting secondary flow patterns were obtained. The results of the investigation indicated the importance of the inlet total pressure profile in determining the development of secondary flows in the vane passage. It was shown that secondary flow vortices of opposite sense to that which are typically observed can occur. Dependence of vortex strength and sense of rotation on stagnation

pressure distribution was clearly illustrated. Unlike the CERTS study described above, distortion of the inlet temperature profile was not presented. However, results of temperature distortion were presented and discussed in a later paper by Hermanson and Thole (2003).

Collectively, these investigations show that the inlet temperature and velocity profiles to a turbine dictate the subsequent secondary flow patterns. In addition, these secondary flows result in a redistribution of flow with the potential of transporting hot gas to flow surfaces. For these reasons, realistic turbine inlet conditions were generated in this investigation through the use of a combustor simulator upstream of the vane cascade. An understanding of the effects of inlet conditions on turbine passage flows and heat transfer is essential in the design of turbines for long life.

2.4 Methods of Secondary Flow Reduction

Several methods of secondary flow reduction in turbine vane and blade passages have been and continue to be the subject of intense investigation. The primary reason that secondary flow reduction is desirable is that significant loss of turbine efficiency is attributable to these flows. According to Sharma and Butler (1987), secondary flow losses can represent as much as 30-50% of the total aerodynamic loss through a vane or blade passage. In addition, the relative importance of secondary flow loss increases as aerodynamic loading increases and aspect ratio decreases. In this section, two approaches to secondary flow reduction will be discussed: endwall contouring and modification of the leading edge/endwall junction. As the motivation behind the latter method was largely derived from the successful demonstration of various filleting concepts in wing/body junctions, a brief review of this motivating work is also given. Most turbine secondary flow reduction studies have been pursued exclusively from the perspective of realizing an aerodynamic benefit, with the exception of one computational study which considered the heat transfer benefits as well.

The use of three-dimensional endwall contouring for secondary flow reduction was investigated computationally by Harvey et al. (1999) and experimentally verified by Hartland et al. (1999). In the computational work by Harvey et al., the effects of endwall perturbations on the flow field were calculated. The results of these calculations were

then put into a linear design system, and using linear superposition theory, many combinations of endwall shape were investigated to arrive at an optimum. The purpose of the linear design system was to reduce the computational cost of arriving at an endwall shape. Next, the resulting endwall design from the linear design system was verified using computational fluid dynamics prior to experimental testing. Significant reduction of secondary flows and exit flow angle deviations were predicted for the contoured endwall, however, the overall reduction in loss was predicted to be small. The results of the experimental verification by Hartland et al. confirm the predicted reduction in secondary flows and exit flow angle deviations, but contrary to the prediction, the measured reduction in secondary flow loss was more significant than predicted at 30%. In conclusion, this work illustrates that endwall contouring is a powerful tool for the reduction of secondary flows, showing aerodynamic improvements comparable to the currently used techniques of differential airfoil skew and compound lean.

Similar to the flow about the leading edge of a turbine airfoil, a horseshoe vortex also forms at the junction between a wing and aircraft fuselage. The two flow situations are directly analogous; therefore, the formation of a horseshoe vortex is not surprising and follows a similar explanation. As the fuselage boundary layer approaches the leading edge of the wing, it encounters a steep adverse pressure gradient causing the boundary layer to separate and roll up into a horseshoe vortex. Also, to no surprise, this vortical flow results in an increase in the interference drag associated with the wing-fuselage junction, and adversely affects the flow on downstream surfaces. In an attempt to prevent the formation of the leading edge horseshoe vortex and thereby alleviate the adverse effects of its presence, researchers have investigated various junction fillets yielding promising results. The work of Zess and Thole (2002) extended the leading edge fillet concept to a turbine vane, with the principal application difference being considerable more flow turning through the vane passage than is achieved with an aircraft wing. However, prior to discussing the research of Zess and Thole, the motivating efforts behind their work merit discussion.

Kubendran and Harvey (1985) investigated the use of a fillet in the leading edge/endwall junction of a symmetric NACA 0012 airfoil to assess the impact of such a modification on the flow field around and downstream of the junction. In the design of

their fillets, they established several basic design criteria based on dimensional arguments. Among these criteria were that the fillet height should not significantly exceed the thickness of the approaching turbulent boundary layer, and that the width or thickness of the fillet should not exceed the maximum thickness of the airfoil. The three fillet configurations tested are illustrated in Figure 2.6, while fillet dimensions relative to boundary layer thickness are provided in Table 2.1. The merit of each fillet design was assessed through analysis of measurements in the wake region of the airfoil. The results of Kubendran and Harvey indicate a reduction in junction drag and improved flow characteristics in the wake region for each leading edge fillet tested. However, slight deterioration of fillet performance was observed from configuration #2 to configuration #3, leading the researchers to hypothesize the existence of an optimum fillet size.

In a subsequent investigation by Kubendran, Bar-Sever, and Harvey (1988), fillet configurations #2 and #3 were further studied with a laminar approach boundary layer. Smoke flow visualization indicated that leading edge flow separation is eliminated by both fillets. In addition, both fillets were found to increase the extent of laminar flow about the junction. However, contrary to the results of the previous turbulent boundary layer study, wake measurements indicated more drag reduction for fillet configuration #3 than for configuration #2.

A computational study of various leading edge fillet designs was conducted by Sung and Lin (1988). Similar to the previously discussed investigations, Sung and Lin applied the fillets to a symmetric airfoil(NACA 0020) at zero angle of attack. The three fillet configurations considered are illustrated in Figure 2.7. Again, based on scaling arguments, the dimensions of the fillets are expressed in terms of boundary layer thickness. The criteria established for fillet effectiveness in this investigation were drag reduction and a reduction in the non-uniformity of the wake velocity profile. The latter criterion was selected citing application to naval systems where non-uniform inflow to a propeller is undesirable. Though all three fillet configurations indicated improvement, configuration #3 was found to be clearly superior to the other two in reducing the non-uniformity of the wake velocity profile. Sung and Lin suggest that the superior performance of fillet #3 may be explained by its similarity to the shape and location of the horseshoe vortex that occurs in the unfilleted junction. Since the distance between

the vortex core and airfoil leading edge is longer than the distance between the vortex core and flat plate, they argue that a fillet having a longer length than height should be expected to perform better than a fillet with a length equal to or shorter than its height. Based on the results of this study, Sung and Lin conclude that an efficient fillet should have a minimum height of one boundary layer thickness and a minimum length of two boundary layer thicknesses.

A combined computational and experimental leading edge fillet investigation was conducted by Sung et al. (1988). In this study, the efficient fillet geometry criteria suggested by Sung and Lin, was applied to two different symmetric airfoil geometries, a NACA 0012 and a NACA 0020. The reason two airfoil geometries were considered was to determine the impact of leading edge radius on fillet effectiveness. For both airfoils, the leading edge fillet was found to be effective in reducing the size and strength of the horseshoe vortex. Perhaps the most important result of this investigation, favorable comparison of the computations with experimental measurements validated the legitimacy of a computational approach in the design of leading edge fillets.

In a two part study by Devenport et al. (1990) and Devenport et al. (1992), two different leading edge fillet geometries were investigated at two different turbulent boundary layer thicknesses. In the first part of the study, a circular fillet of constant radius around the entire base of a symmetric airfoil was considered, as illustrated in Figure 2.8. Unfortunately, this fillet did not prevent leading edge separation of the boundary layer associated with the development of the horseshoe vortex. To the contrary, the circular fillet appeared to amplify the size and strength of the vortex structure, in addition to enhancing the unsteadiness of the vortex legs in the downstream wake. In the second part of this study, a fillet more akin to that of Sung et al. (1988), in terms of length to height ratio, was considered. However, unlike Sung et al., Devenport at al. (1992) designed their fillet, shown in Figure 2.9, to smoothly transition into the airfoil leading edge and upstream endwall, on the belief that this would enhance performance. At zero angle of attack, this fillet eliminated boundary layer separation and prevented the formation of a horseshoe vortex. Additional fillet benefits cited include a reduction in the magnitude of surface pressure fluctuation about the airfoil, and a reduction in the non-uniformity of the wake velocity distribution.

Additional investigations of leading edge fillets on symmetric airfoils were conducted by Pierce et al. (1988) and Bernstein and Hamid (1996). Pierce et al. considered a triangular fillet with a sharp leading edge, shown in Figure 2.10, for hydrodynamic performance enhancement of marine appendages. As a testament to the effectiveness of fillets in marine applications, the new Seawolf class of submarines feature a fillet on the leading edge of the conning tower, as shown in Figure 2.11. Bernstein and Hamid investigated the use of an asymmetric strake-like fillet in the wing-body junction of a swept wing as illustrated in Figure 2.12.

Motivated by the success of fillet application in external aerodynamic applications, Zess and Thole (2001) investigated such a modification to the leading edge/endwall junction of a turbine vane. Through application of a leading edge fillet, these researchers sought to preclude formation of the horseshoe vortex, and thereby reduce vane passage secondary flows and associated losses. Computational fluid dynamics was used as a design tool to investigate different fillet concepts. Zess and Thole computationally investigated nine different leading edge fillet geometries prior to selecting a design for experimental verification. The fillet selected for testing is illustrated in Figure 2.13. To understand the mechanism by which the fillet prevents the development of the horseshoe vortex, one must first understand what drives the formation of the vortex. As previously discussed in section 2.1, horseshoe vortex development is driven by the radial total pressure gradient that exists due to the inlet boundary layer. The fillet acts to accelerate the boundary layer, thereby flattening the total pressure profile at the vane leading edge and preventing development of the horseshoe vortex. Upon completion of the computational design, flow field measurements were taken to verify fillet performance. Excellent agreement between the computational and experimental results was observed with the fillet effectively eliminating the horseshoe vortex. The success of Zess and Thole directly provided the motivation for the work presented herein.

A more recent computational study by Shih and Lin (2002), investigated the use of a leading edge fillet and inlet swirl to control secondary flows in a vane passage. Two different fillet geometries and a no fillet baseline were considered for three different inlet swirl configurations: no swirl and swirls of opposite rotation with linearly varying swirl

angle from endwall to endwall. The two fillets differed in how they blended into the vane geometry with one fading into the vane surface and the other fading into the endwall as shown in Figures 2.14 and 2.15, respectively. For both fillets, the point of maximum height above the endwall coincided with the vane stagnation location. No other specifics or mathematical description of the fillet geometries were given.

Solutions to the flow field and heat transfer in the vane passage were calculated using a code developed at NASA Langley Research Center called CFL3D. The solution domain for this investigation models the entire vane span with one flat endwall and one contoured (contracting) endwall upstream of the leading edge. A structured grid generated for the solution domain enabled modeling all the way to the wall, with the first five grid points within a y^+ of 5. The applied inlet boundary condition consists of uniform temperature (300 K) air and a one-seventh power-law(turbulent) streamwise velocity profile. For cases with inlet swirl, a profile for the tangential component of velocity is superimposed. The endwall and vane surfaces were modeled as constant temperature (270 K) in the computations.

To directly compare the aerodynamic and heat transfer performance of each fillet/swirl combination, Shih and Lin calculated integrated results of average total pressure drop and net surface heat transfer rate for each simulation. In comparison to the baseline no fillet and no swirl case, all simulated cases with inlet swirl and/or a leading edge fillet showed improvements in both total pressure drop and surface heat loads. Percent reductions in total pressure drop ranged from 38.0 to 44.5%. Endwall heat load results indicate reductions between 32.9 and 45.3% for the contoured endwall and reductions between 32.4 and 44.5% for the flat endwall. Vane surface heat load reductions were found to be less substantial, between 12.0 and 19.1%. While no single case provided maximum reduction for every metric, a case with inlet swirl and no fillet came very close to doing so. In comparison, the aerodynamic and heat transfer benefits realized for cases with fillets and no inlet swirl were not as great. Shih and Lin conclude that both inlet swirl and leading-edge fillets can effectively reduce aerodynamic loss and surface heat transfer.

A slightly different modification to the leading edge/endwall junction of a turbine blade was studied by Sauer et al. (2000). These researchers investigated the application

of a leading edge "bulb", shown in Figure 2.16, for endwall loss reduction. Similar to a fillet, the bulb locally alters the geometry of the blade leading edge in the region adjacent to the endwall, however, the transition between the bulb and endwall remains a sharp rectangular corner. Contrary to the design intent of a fillet, the bulb was not designed to reduce the strength of the secondary flows. Rather, the leading edge bulb was designed to increase the strength of the suction side leg of the horseshoe vortex, and thereby affect a change in location of the passage vortex away from the suction surface. The mechanism for endwall loss reduction was to reduce the interaction of the passage vortex with the airfoil suction side boundary layer. For the best bulb design, Sauer et al. measured a 47% reduction in endwall losses. Computational fluid dynamics results qualitatively agreed to their experimental measurements, however, no flow field measurements within the blade passage were presented for comparison.

Becz et al. (2003) experimentally investigated the influence of two leading edge bulb geometries, similar to that presented by Sauer et al. (2000), and a fillet geometry, similar to that of Zess and Thole (2002), on endwall loss through a turbine blade cascade. Total pressure loss measurements were performed for four leading edge configurations: a baseline configuration, a small and a large bulb geometry, and a leading edge fillet. Though the large bulb produced a slight increase in total loss, both the small bulb and the leading edge fillet reduced the total area-averaged loss by 8%, with a 15% reduction in secondary flow loss. Though yielding remarkably similar loss reductions, the small bulb and fillet results gave indication that the mechanisms by which each is affecting the flow is possibly different, leading to the author's assertion that the geometries may be combined in some way to yield an optimum leading edge junction shape.

2.5 Literature Review Conclusions and Uniqueness of this Investigation

Three important conclusions can be drawn from the literature review. First, past investigations of the impact of passage secondary flows on heat transfer clearly show that the presence of these flows result in significant augmentation of the local heat transfer coefficient on the passage endwall. Second, secondary flow development is dependent on the inlet boundary conditions to a vane or blade passage, stressing the importance of specifying these conditions as accurately as possible. Finally, several different

techniques of secondary flow reduction have been investigated, however, with exception to the study by Shih and Lin (2002), only the aerodynamic benefits of these techniques have been considered. At the inception of the investigation reported herein, it was believed that a heat transfer benefit could be derived from the implementation of a leading edge fillet, and that this benefit would perhaps have far greater impact on gas turbine development than aerodynamic considerations alone. Thus, the objective of this investigation was to optimize the shape of a vane leading edge fillet to maximize the thermal benefit. Unique to this investigation and coupled to the optimization approach was the use of realistic boundary conditions. Understanding the importance of boundary conditions, realistic combustor exit profiles were utilized in both the computational and experimental research efforts with the aid of a combustor simulator.

In summary, a unique approach to the aerothermal design of a turbine vane leading edge fillet was undertaken. Rather than focusing on the aerodynamic benefits, this study considered the optimization of a leading edge fillet to maximize the heat transfer benefits. The potential benefits of this design approach include a decrease in the necessary amount of turbine cooling flow, an increase in the maximum allowable turbine inlet temperature, an increase in turbine life, and a reduction in total pressure loss through the vane. Since this approach includes the thermal aspects of turbine component design, it is believed that this approach will prove to be superior to focusing on secondary flow reduction alone.

Table 2.1 Summary of previous fillet investigations (adapted from Zess and Thole (2002)).

Investigator	Geometry	Fillet Length	Fillet Height
Kubendran and Harvey (1985)	Fillet Configuration #1: Curved Fillet Configuration #2: Linear Fillet Configuration #3: Linear	1.8δ 1.8δ 3.6δ	1.8δ 1.8δ 1.8δ
Kubendran et al. (1988)	Fillet Configuration #1: Linear Fillet Configuration #2: Linear	3.7δ 7.4δ	3.7δ 3.7δ
Pierce et al. (1988)	Triangular Fillet w/ Sharp Leading Edge	0.8δ	2.3δ
Sung and C.-W. Lin (1988)	Fillet Configuration #1: Linear Fillet Configuration #2: Linear Fillet Configuration #3: Linear	1δ 1δ 2δ	1δ 1.5δ 1δ
Sung et al. (1988)	Linear Fillet (2 NACA symmetric airfoils)	2δ	1δ
Devenport et al. (1990)	Constant Radius Fillet (2 b.l. thicknesses)	1.1δ 2.1δ	1.1δ 2.1δ
Devenport et al. (1992)	Curved Fillet (Strake) (2 b.l. thicknesses)	4.3δ 8.4δ	2δ 3.8δ
Bernstein and Hamid (1996)	Asymmetric Curved Fillet	3.3δ	3.3δ
Sauer et al. (2001)	Leading Edge Bulb	no data	no data
Zess and Thole (2002)	Asymmetric Linear Fillet	2δ	1δ
Shih and Y.-L. Lin (2002)	Vane-Blended Linear Fillet Endwall-Blended Linear Fillet	no data no data	no data no data

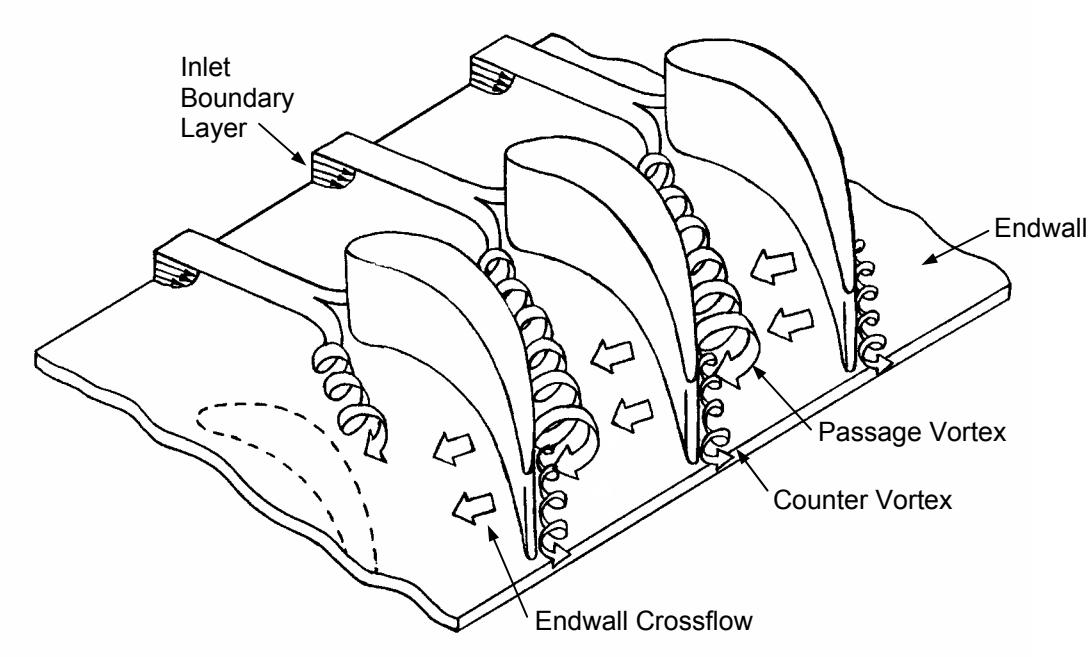

Figure 2.1 Secondary flow model presented by Langston (1980).

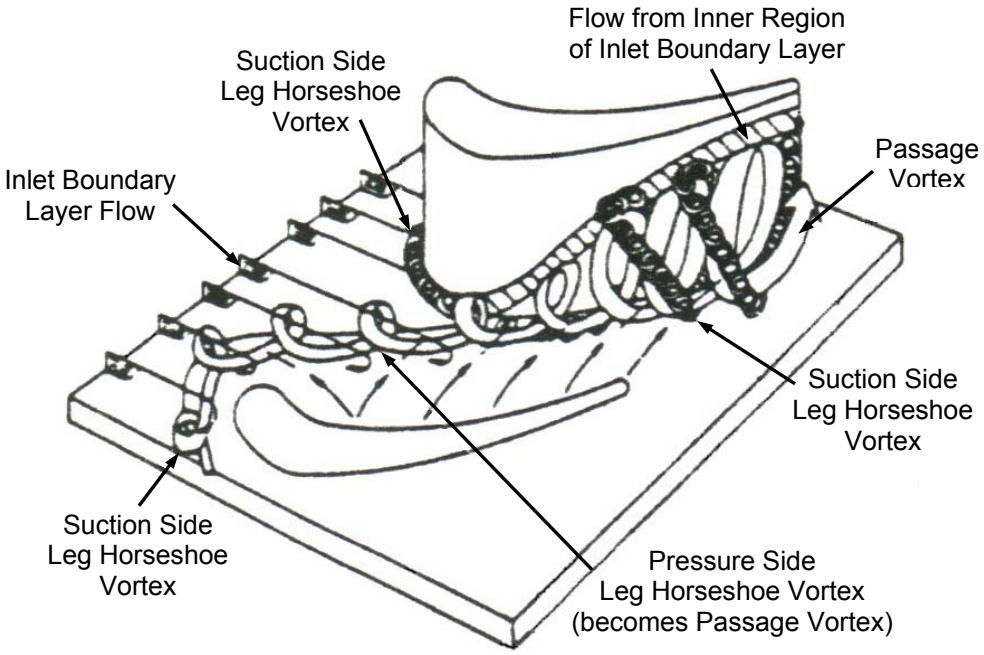

Figure 2.2 Secondary flow model presented by Sharma and Butler (1987).

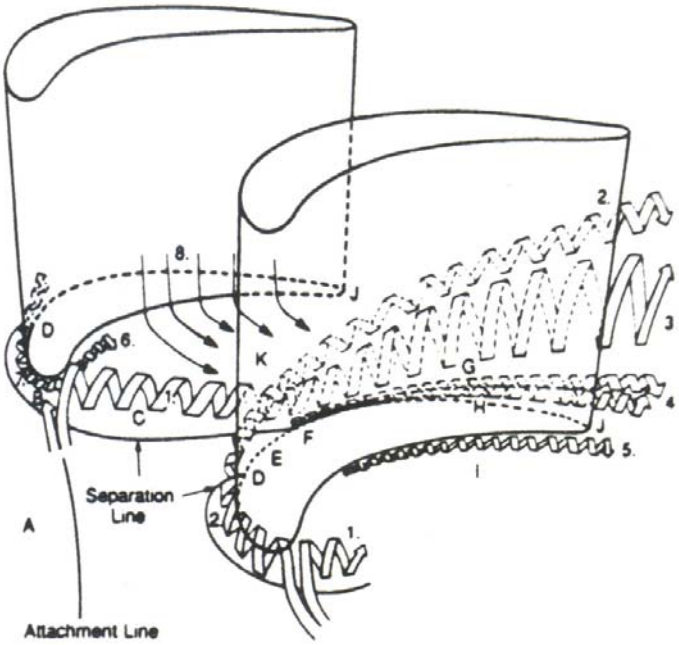

1. Leading edge pressure side vortex
2. Leading edge suction side vortex
3. Passage vortex
4. Suction side corner vortices
5. Pressure side corner vortex
6. Pressure side leading edge corner vortex
7. Suction side leading edge corner vortex
8. Downward velocity component on pressure side

Figure 2.3 Secondary flow model developed by Goldstein and Spores (1988).

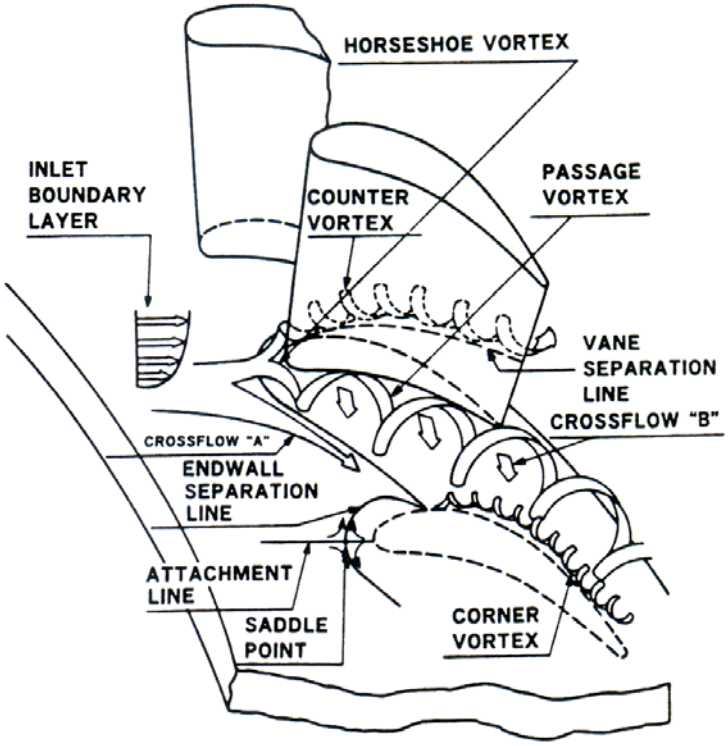

Figure 2.4 Secondary flow model presented by Takeishi, et al. (1990).

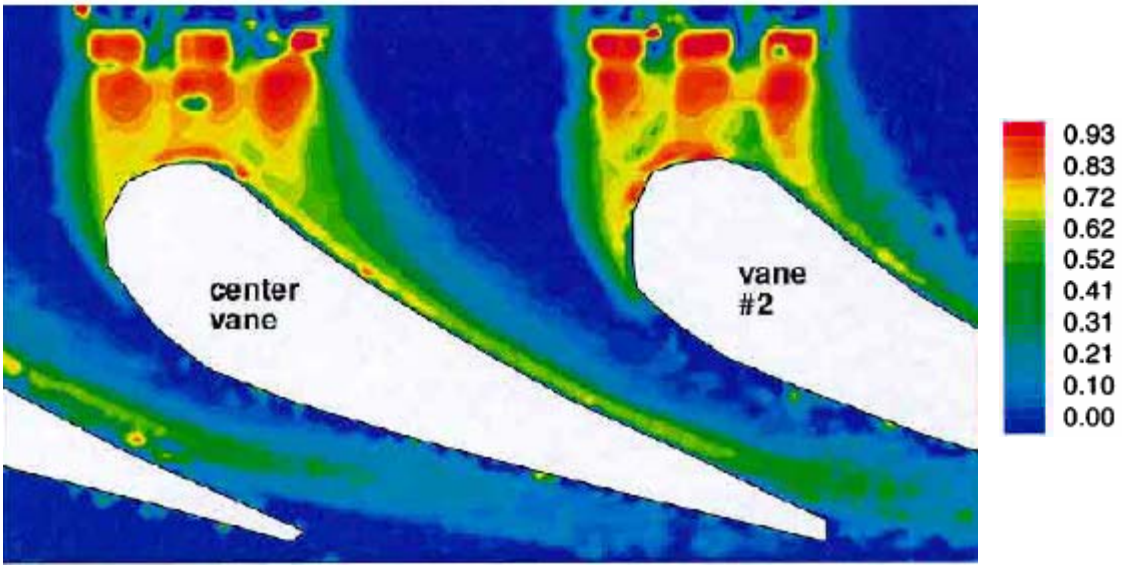

Figure 2.5 Endwall cooling effectiveness distribution as measured by Roy et al. (2000) with cooling air injection through three leading edge slots.

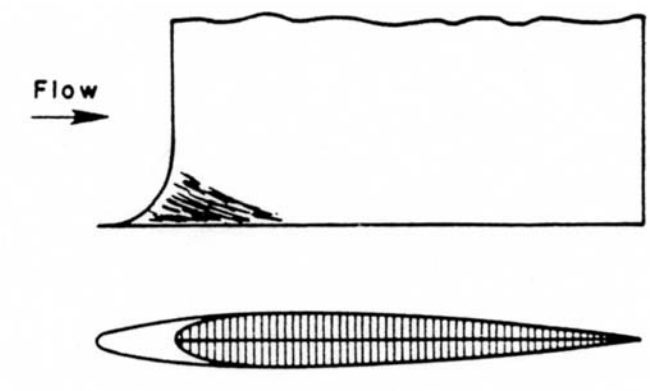

Configuration #1

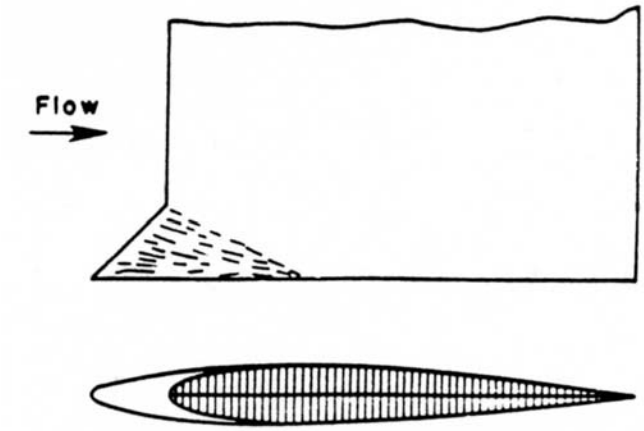

Configuration #2

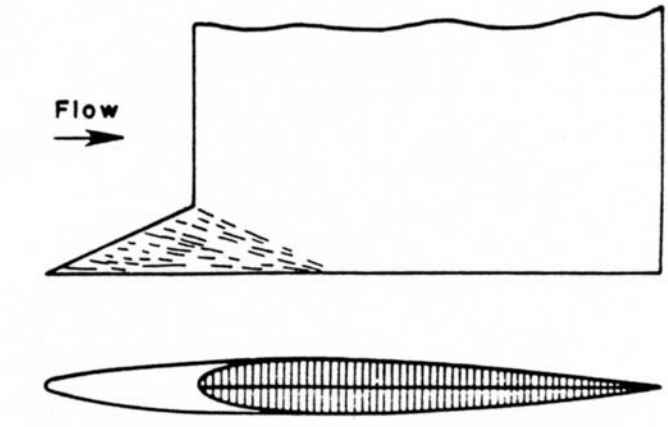

Configuration #3

Figure 2.6 Leading edge fillet geometries investigated by Kubendran and Harvey (1985).

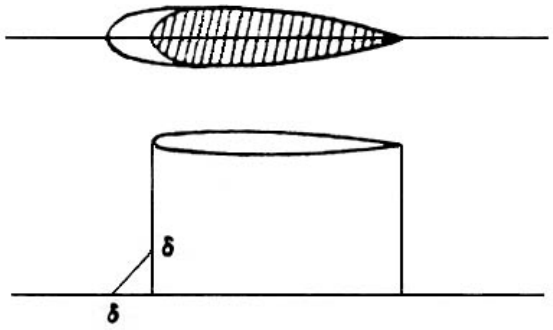

Configuration #1

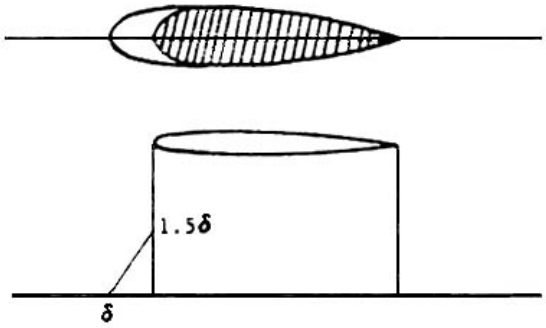

Configuration #2

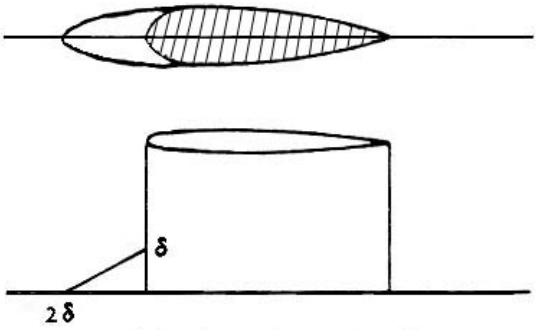

Configuration #3

Figure 2.7 Leading edge fillet geometries considered in the numerical investigation of Sung and Lin (1988).

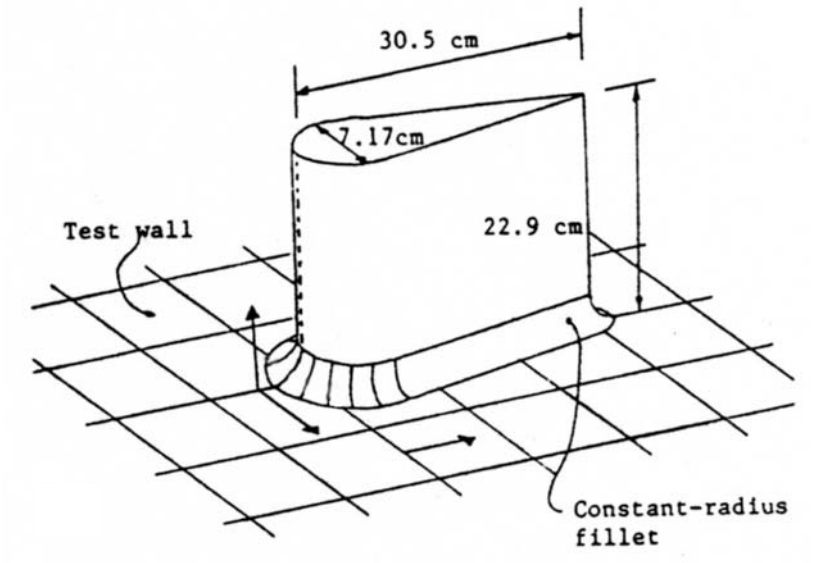

Figure 2.8 Constant radius fillet investigated by Devenport et al. (1990).

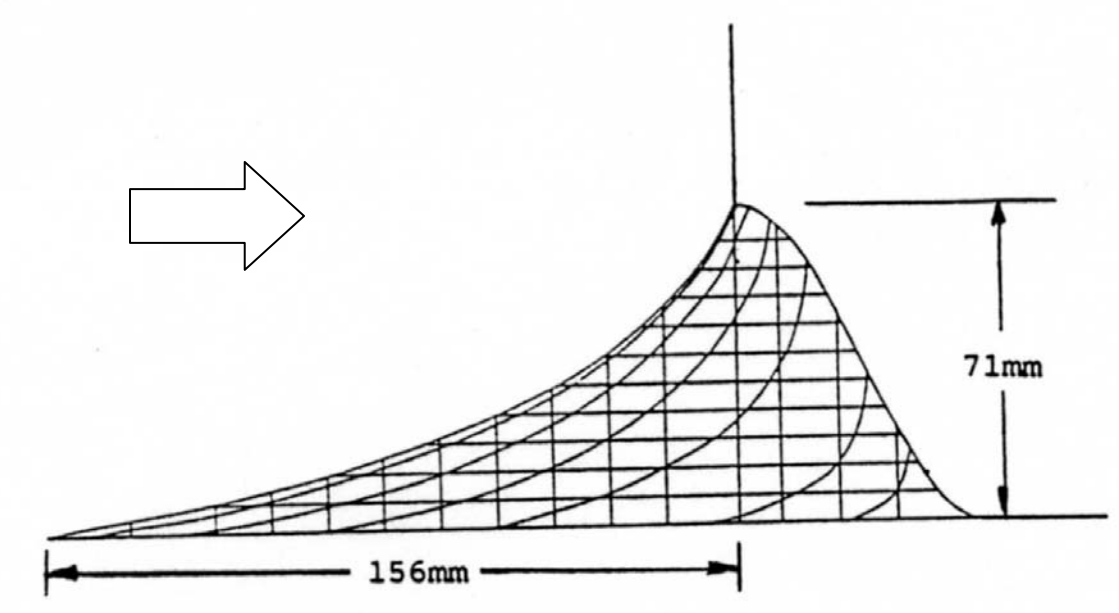

Figure 2.9 Curved leading edge fillet(strake) investigated by Devenport et al. (1992).

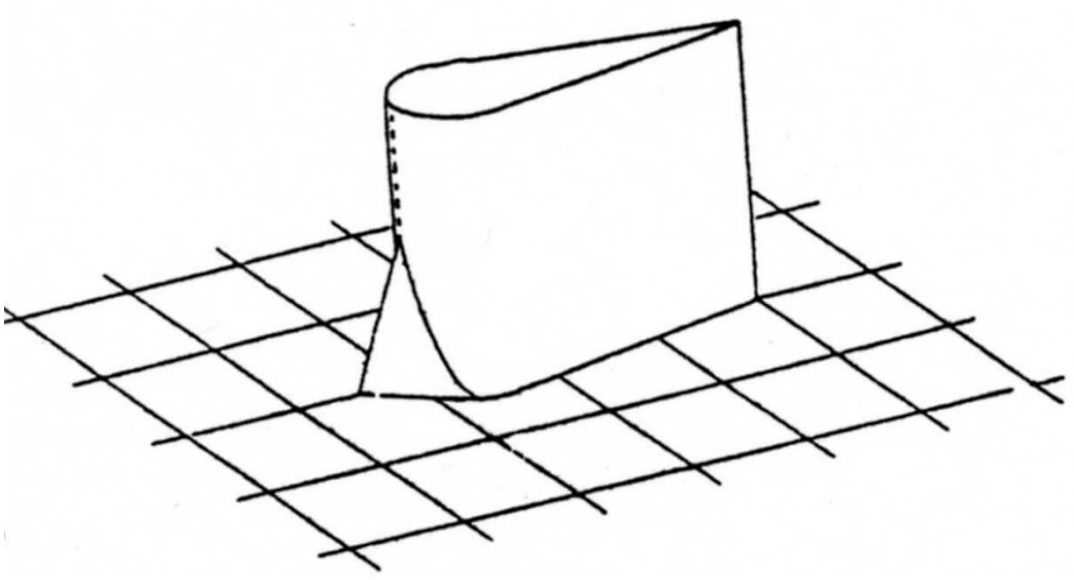

Figure 2.10 Triangular fillet with sharp leading edge studied by Pierce et al. (1988).

Figure 2.11 Fillet on the leading edge of a Seawolf class submarine conning tower.

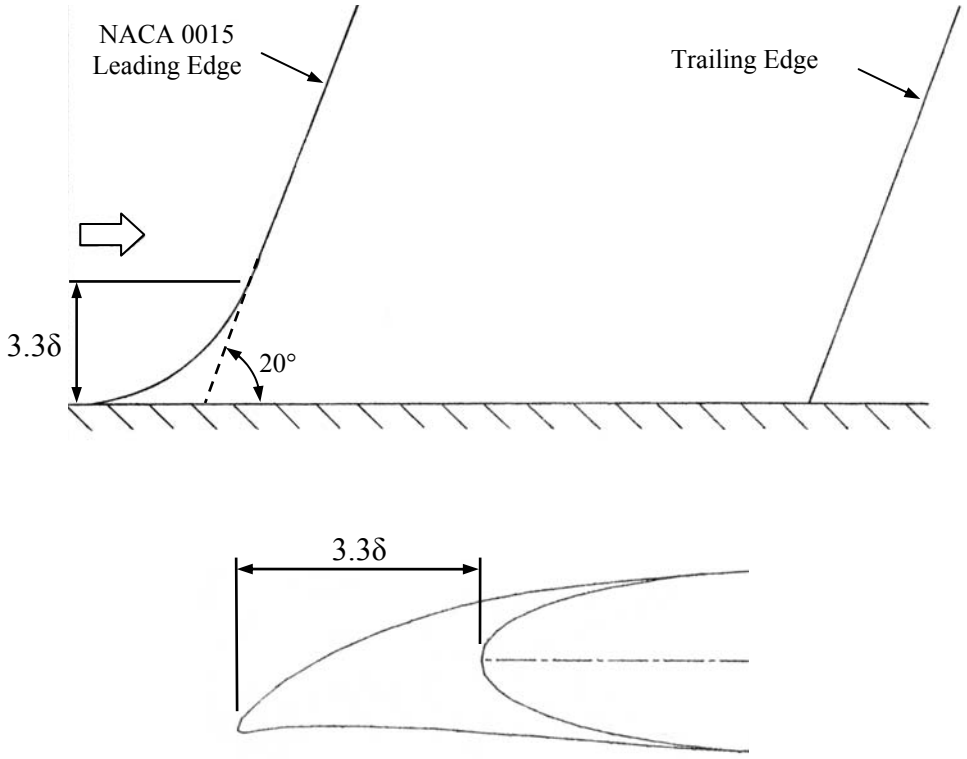

Figure 2.12 Side view and top view of the asymmetric fillet investigated by Bernstein and Hamid (1996).

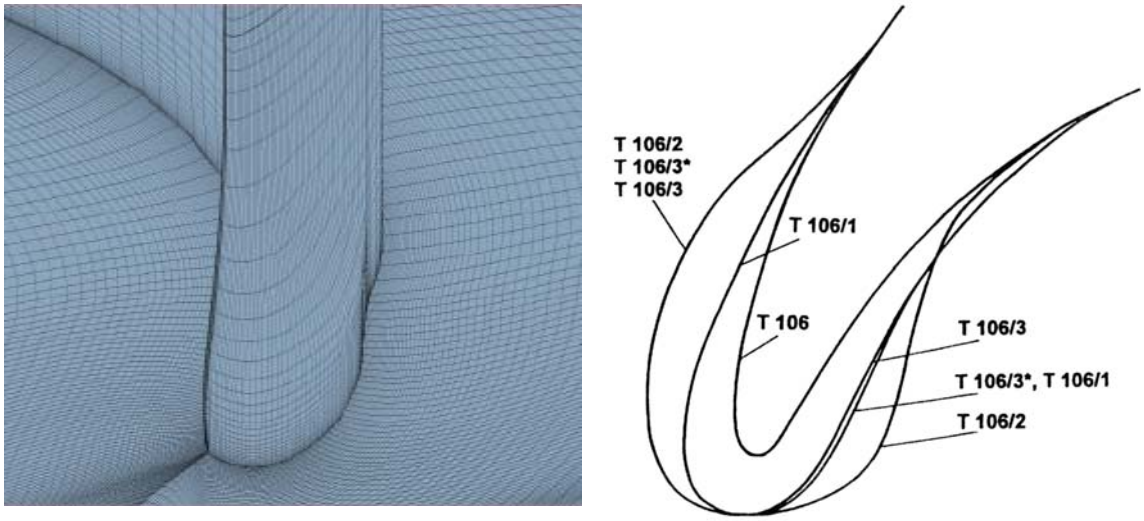

Figure 2.13 Leading edge bulb geometries studied by Sauer et al. (2000).

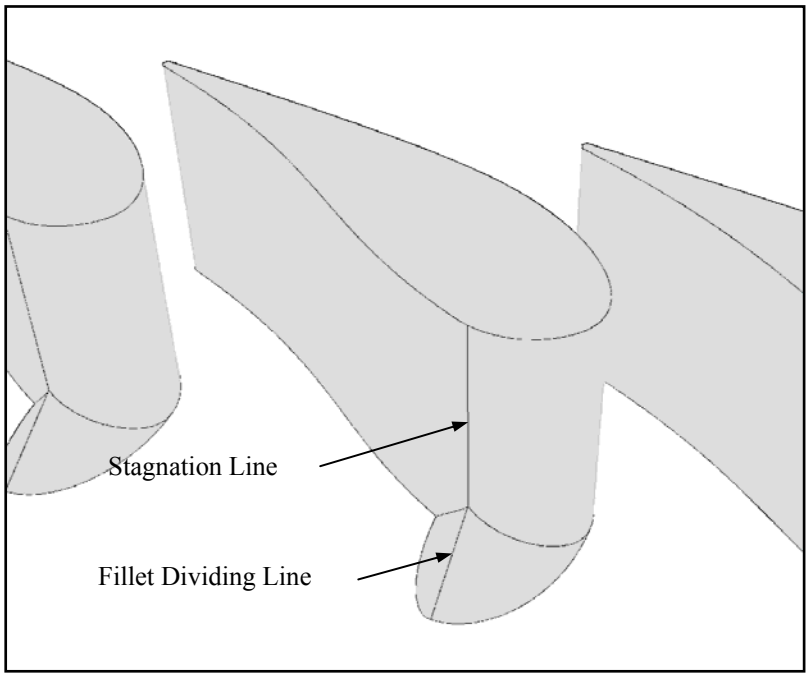

Figure 2.14 Computationally designed and experimentally verified leading edge fillet of Zess and Thole (2002).

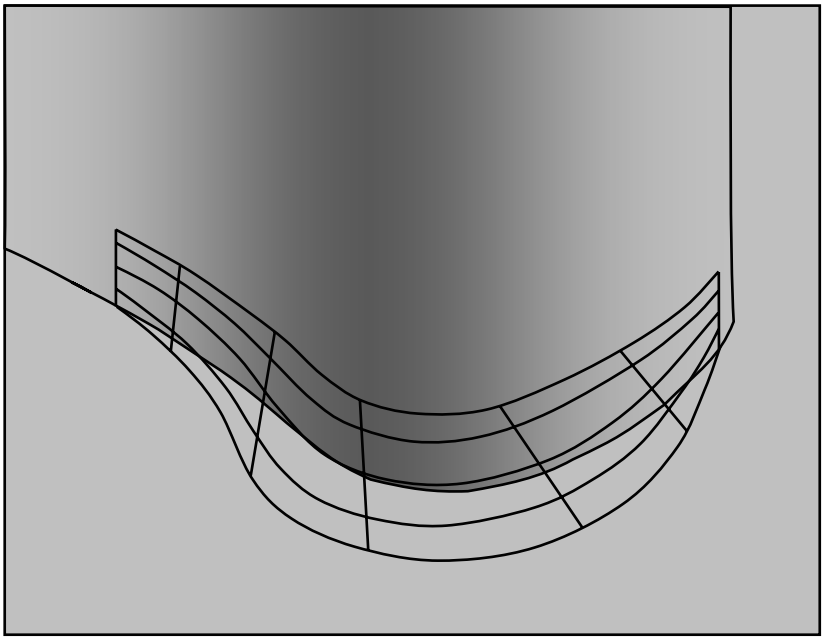

Figure 2.15 Vane-blended linear fillet investigated computationally by Shih and Lin (2002).

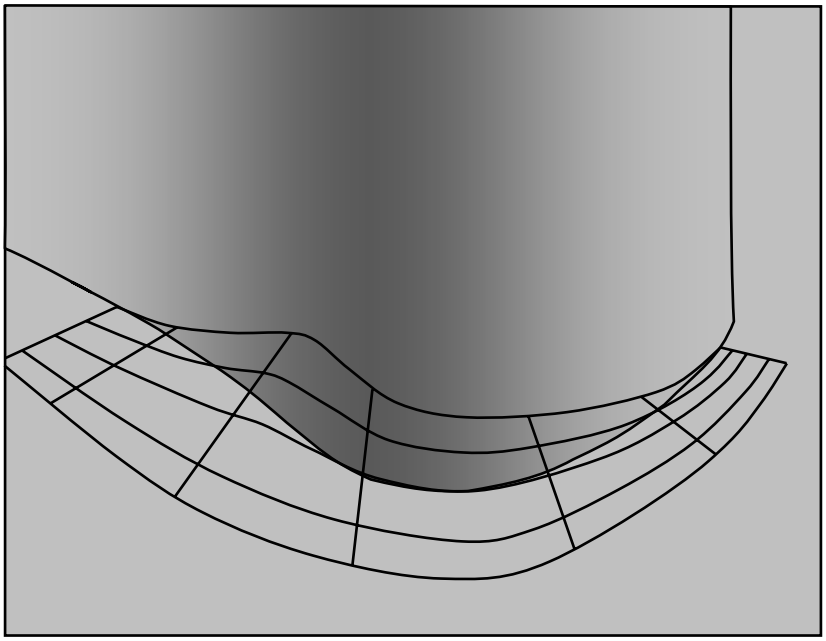

Figure 2.16 Endwall-blended linear fillet investigated computationally by Shih and Lin (2002).